Centrifuge and real-time hybrid testing of tunnelling beneath piles and piled buildings

Andrea Franza[1] and Alec M. Marshall[2]

[1]Research Associate, Department of Engineering, University of Cambridge, UK. Formerly, Faculty of Engineering, University of Nottingham, UK. Email: andreafranza@gmail.com

[2]Associate Professor, Faculty of Engineering, University of Nottingham, UK. Email: alec.marshall@nottingham.ac.uk

ABSTRACT

Tunnels are constructed increasingly close to existing buried structures, including pile foundations. This poses a serious concern, especially for tunnels built beneath piles. Current understanding of the global tunnel-soil-pile-building interaction effects is lacking, which leads to designs which may be overly conservative or the adoption of expensive measures to protect buildings. This paper presents outcomes from 24 geotechnical centrifuge tests that aim to investigate the salient mechanisms that govern piled building response to tunnelling. Centrifuge test data include greenfield tunnelling, pile loading, and tunnelling beneath single piles and piled frames, all within sand. The global tunnel-piled frame interaction scenario is investigated using a newly developed real-time hybrid testing technique, wherein a numerical model is used to simulate a building frame, a physical (centrifuge) model is used to replicate the tunnel-soil-foundation system and structural loads, and coupling of data between the numerical and physical models is achieved using a real-time load-control interface. The technique enables, for the first time, a realistic redistribution of pile loads (based on the superstructure characteristics) to be modelled in the centrifuge. The unique dataset is used to quantify the effects of several factors which have not previously been well defined, including the pile installation method, initial pile safety factor, and superstructure characteristics.

In particular, results illustrate that pile settlement and failure mechanisms are highly dependent on the pre-tunnelling loads and the load redistribution that occurs between piles during tunnel volume loss, which are related to structure weight and stiffness. The paper also provides insight as to how pile capacity should be dealt with in a tunnel-pile interaction context.

INTRODUCTION

The expansion of cities causes increased demands for underground infrastructure and the need to construct tunnels in the proximity of man-made assets. Excavation-induced ground movements and stress relief may adversely affect existing pile foundations and associated superstructures. In particular, tunnelling beneath piles can result in differential pile settlements and, potentially, pile failure.

Research has provided empirical approaches, simplified analytical methods, and numerical analyses for the prediction of settlements and loss of capacity of existing piles due to tunnel excavation (Basile 2014; Devriendt and Williamson 2011; Jacobsz et al. 2004; Hong et al. 2015; Marshall 2012; Marshall and Haji 2015; Selemetas and Standing 2017; Soomro et al. 2015). However, few studies have recognized the importance of pile safety factor (Dias and Bezuijen 2015; Lee and Chiang 2007; Williamson et al. 2017b; Zhang et al. 2011) and the role of pile installation method (displacement versus non-displacement piles). In addition, the impact of the superstructure action on tunnelling-induced displacements of piles and the resulting deformations has received limited attention (Franza et al. 2017; Franza and Marshall 2018). These aspects require further investigation.

Physical modelling using a geotechnical centrifuge has been used to investigate many of the mechanisms related to tunnel-pile foundation interaction (Jacobsz et al. 2004; Lee and Chiang 2007; Loganathan et al. 2000; Marshall and Mair 2011; Ng et al. 2013; Ng et al. 2014; Williamson et al. 2017b; Williamson et al. 2017a). Conventional centrifuge testing tends to break the problem down into discrete parts (e.g. isolated piles) and/or to use simplified superstructures (e.g. constant loads from the superstructure, rigid connections, beams). However, a complete replication of soil-structure systems can not be obtained when the structural and geotechnical domains are decoupled, and the use of a simplified superstructure limits the analysis and may significantly alter the soil-structure interactions.

Complex soil-structure interaction (SSI) problems can be studied through real-time hybrid models whereby the real-time sub-structure testing approach described by Blakeborough et al.

(2001) is implemented: a physical test (modelling a key portion of the domain) and a numerical simulation (modelling the remaining domain) are run simultaneously, while shared boundary conditions are exchanged at a real-time frequency. Hybrid modelling of tunnel-building interaction using a reduced-scale centrifuge model is described in this paper and is referred to as coupled centrifuge-numerical modelling (CCNM). The feasibility of hybrid modelling using a geotechnical centrifuge has been demonstrated by recent pioneering works (Franza et al. 2016; Kong et al. 2015; Idinyang et al. 2018).

SCOPE OF WORK

This paper aims to illustrate the effects of installation method, initial safety factor, and load redistribution due to frame action on tunnelling-induced settlements of axially loaded pile foundations as well as the resulting superstructure deformations. Data are provided from a series of geotechnical centrifuge tests of tunnel excavation beneath piles and piled frames in dry silica sand, including both conventional and CCNM test methods. In the following, all results are presented in model scale unless otherwise stated.

TEST DETAILS

A total of 24 tests were performed at 60g (i.e. acceleration scaling factor $N = 60$) using the University of Nottingham Centre for Geomechanics centrifuge, as listed in Table 1, which provides details on pile load condition, geometry, and configuration. Tests are grouped into 4 categories: series A is a greenfield test; series B are pre-tunnelling single pile loading tests (non-displacement piles); series C investigated the response of isolated piles to tunnelling; and series D modelled the response of piled frames to tunnelling, applying the CCNM technique. Tests are labelled according to installation method (N = non-displacement, D = displacement), pile position (see Figure 1), and initial safety factor (for instance N2SF1.5 represents a non-displacement pile located in position 2 with an initial safety factor of 1.5); the G indicates pile group and FR denotes the structural frame, which is discussed below.

The layout of series B, C and D tests are sketched in Figure 1(a), (b) and (c), respectively. In series C, displacement and non-displacement piles in positions 1-3 were tested. Service loads

were applied (kept constant with tunnel volume loss, $V_{l,t}$) such that the initial safety factor SF_0 was either 1.5 or 2.5. Note that only piles in positions 1 and 2 have their tips within the influence zones defined by Jacobsz et al. (2004) where large pile settlements caused by tunnelling are expected.

In series D, tests were performed for a transverse row (positions 1-4) of displacement or non-displacement piles representing the foundation of a framed building. Four superstructures were considered, in which only the structural stiffness was varied; superstructure weight was kept constant in all series D tests. The prototype superstructure consisted of an 8 storey concrete frame (E = 30GPa) with a storey height, h, and a span length, S_t, of 3m and 4.5m, respectively. In Table 1, FR00 indicates a fully flexible frame, whereas FR30, FR50, and FR70 indicate frames of increasing stiffness with beam and column elements having square cross-sections of 0.3×0.3, 0.5×0.5, and $0.7 \times 0.7\text{m}^2$, respectively. The frame was assumed linear elastic with fixed column-beam connections. The tests only consider vertical pile loads and settlements in the centrifuge, which are the most influential parameters for this problem (as discussed by Franza et al. (2017)). This implies a hinged connection between the pile cap and the base of a column, which does not necessarily reflect reality but has been found to have a secondary effect on results. For example, from the model of the frame FR50 (detailed later in the text), the reaction force measured at position 1, $R_{z,1}$, was obtained by varying the boundary conditions at positions 1-4 (refer to Figure 1(c)). By imposing a settlement of 10mm at position 1 while fixing all locations (vertical, horizontal, and rotational degrees of freedom (DOF)), a value of $R_{z,1}$ = 634kN was obtained. By releasing the rotational DOF at positions 1-4, a value of $R_{z,1}$ = 621kN was obtained (2.1% difference), and the changes in vertical reaction forces at positions 2-4 were all less than 3%.

In test series D, initial service loads, P_0, could have been assessed for each pile using either a specific structural analysis accounting for the frame loading or the frame construction stages. However, the adopted approach (a uniform distribution of P_0) allows isolating the influence of the load redistribution due to building action without adding further complexity to the problem (e.g. the effects of varying pre-tunnelling pile loads among the pile group on the tunnel-pile interaction (TPI) has not been investigated by previous research). For the piled frame, building weight P_0

resulted in $SF_0 = 1.5$ and 2 for non-displacement and displacement piles, respectively, which are in the range of typical design values.

COUPLED CENTRIFUGE-NUMERICAL MODELLING (CCNM)

This section presents the CCNM methodology (Franza et al. 2016; Idinyang et al. 2018) adopted in this study, as illustrated in Figure 2(a). A numerical model simulates the superstructure whereas the geotechnical domain (tunnel, ground, foundation, and structural loads) is replicated within the centrifuge. Shared boundary conditions, achieved using a real-time data acquisition and load-control interface (Idinyang et al. 2018), are illustrated in Figure 2(b).

The CCNM methodology can be summarized as follows. [1] The model piles are driven and/or loaded in-flight with service loads, P_0. [2] The numerical model is started; physical and numerical models are coupled by the real-time interface through continuous and high-speed [a] transfer of incremental pile displacements, u_z, measured in the centrifuge to the numerical model, [b] retrieval of target loads, P', obtained from the latest numerical simulation, and [c] adjustment of the pile loads in the centrifuge, P, to the target values, P'. [3] Increments of tunnel volume loss, $\Delta V_{l,t}$, are induced in the model tunnel, causing pile settlements, u_z. Associated superstructure deformations result in pile load changes (i.e. $P' \neq P_0$). Increments of $\Delta V_{l,t}$ are kept small and only applied once a stable state is achieved within the coupled centrifuge-numerical model. Franza et al. (2016) illustrated that this hybrid model is stable in-flight and its load-control performance is satisfactory for this application.

Centrifuge model

The centrifuge equipment is shown in Figure 3 and is based on a tunnelling model for plane-strain greenfield conditions (Zhou et al. 2014). A 90mm diameter model tunnel buried at 225mm depth (at axis) within dry sand was used to replicate a prototype 5.4m diameter tunnel with 13.5m of cover (cover-to-diameter $C/D = 2$). The sand was Leighton Buzzard Fraction E which has an average grain size $D_{50} = 0.12$mm, a specific gravity G_s=2.65, maximum (e_{max}) and minimum (e_{min}) void ratios of 1.01 and 0.61, respectively, and a critical state friction angle $\phi_c \approx 30°$. The tunnel comprised a cylindrical latex membrane filled with water. To replicate in-flight tunnel

volume loss, $V_{l,t}$, a controlled volume of water was extracted from the model tunnel using a tunnel volume control system (comprising constant-head standpipe, solenoid valve, linear actuator, water-filled sealed cylinder, and Linear Variable Differential Transformers (LVDT)) shown in Figure 3(a). This process was conducted up to either pile failure or $V_{l,tmax} = 10\%$. During the greenfield test, the GeoPIV image-based measurement technique was used to measure tunnelling-induced soil displacements at the Perspex window (White et al. 2003).

For the tests investigating tunnelling beneath piles, a foundation consisting of either a single pile or four piles was used. All piles were located along the centre of the container width. A view of the model pile and pile cap is illustrated in Figure 4. A load cell was installed at each pile head to have a reliable measurement of the head load, P. LVDTs were used to measure pile settlements u_z.

Model piles were made from 12mm diameter full section cylindrical aluminium rod with a total length of 185mm and a 60° tip. A fully rough interface was obtained by bonding sand to the periphery of the piles, giving a final diameter, d_p, of 13mm. A threaded hole was made in the top of the pile to allow attachment of a pile cap.

Pile caps were composed of two aluminium round connectors, a load cell, a plate for the LVDT armature, and a loading bar (see Figure 4). Each of the pile loading bars could be loaded/jacked independently using a four-axis servo actuator apparatus and lever system. Four L03 MecVel ballscrew actuators, shown in Figure 3(a), with 100mm stroke and 5kN capacity (at $1g$) were used. As shown in Figure 3(b), a heavy duty die-spring (stiffness rate 155N/mm) was placed inside each actuator cap to damp the pile load-actuator displacement relationship. The actuator caps were fixed to linear guide carriages to ensure vertical travel. Note that the loading system is only able to apply an axial load to the piles. The lever system illustrated in Figure 3(c) was made using 4 aluminium beams and a frame to transfer the action of the actuators to the pile loading bars. Figures 3(c) and (d) show the gantry used to hold the LVDTs and the guides used to ensure the verticality of the pile loading bars, thus preventing the transfer of bending moments by the lever system to the pile caps.

Numerical model

A simple and computationally efficient matrix stiffness method structural analysis based on the finite element method was performed in MATLAB to simulate the frame, adopting a first-order elastic analysis (i.e. the equilibrium analysis is performed for the undeformed configuration and geometric non-linearity, such as P-delta effects, is not considered). At prototype scale, the stiffness matrix of the framed structure, K, was obtained using Euler-Bernoulli beam theory for fixed column-beam connections. Hinged pile-superstructure connections were assumed to replicate the conditions in the centrifuge model (i.e. no bending moments transferred from superstructure to pile). Note that the CCNM methodology can accommodate more rigorous structural numerical analyses (e.g. considering structural damage/non-linearity). The results presented here represent the first phase of testing of the developed CCNM application and provide important reference data for future testing that will explore the effects of structural non-linearity.

Real-time interface

The real-time interface was designed to efficiently carry out the actuator control and data acquisition tasks (full details presented in Idinyang et al. (2018)). It consists of a Field Programmable Gate Array (FPGA) controller for scalable hardware integration, interchangeable modules (for acquisition, relay triggering, motor control, and limit switch sensing), and a local computer that runs LabVIEW. The FPGA controller and its hardware components were mounted on the centrifuge platform adjacent to the model container to minimize noise in the signals.

The main processes that couple the physical and numerical models are contained within two loops that are run independently and at different rates (see Figure 2(a)). The LabVIEW program loop (on the PC) runs at a fixed time interval of 60ms (17Hz), which was found to be satisfactory for this application. This loop [a] monitors changes to the user interface; [b] gets centrifuge model sensor information from the FPGA; [c] feeds incremental pile settlements u_z to the numerical model, which runs as a component of the LabVIEW program using a MathScript node; [d] executes the structural analysis that computes new target loads; and [e] transfers the new target loads to the FPGA. The FPGA program loop, which runs at a real-time frequency ($\approx$ 500Hz), [a] acquires

data from the centrifuge sensors; and [b] adjusts the pile loads in the centrifuge, P, to the target values, P', by performing automatic load-control using a Proportional, Integral, Derivative (PID) algorithm.

To facilitate a range of centrifuge test requirements, the interface could switch between [i] 'manual displacement-control mode' (for pile installation) to execute extension/retraction of the actuators, and [ii] 'automatic load-control mode' to actuate, through the PID control algorithm, either user-defined load demands or target forces P' provided by the numerical model.

Finally, effective LVDT signal filtering was required to avoid unrealistic fluctuations of the target load P'. Signal noise from the centrifuge model is amplified by the scaling factor (N) in the data passed to the numerical model (simulating at prototype scale). Target load at model scale is $P' = K[N(u_z^r + u_z^e)]/N^2$ for a given prototype structure with stiffness K, where u_z^r and u_z^e are the model pile settlements and the error in the LVDT measurement due to signal noise, respectively (both at model scale). Target load fluctuations due to LVDT signal noise are $P'^e = K\ u_z^e/N$. This aspect becomes more critical as superstructure stiffness K increases. The consequences of this is that the CCNM application can run into stability issues when analysing very stiff superstructures; examples of this are presented later in the paper.

MODEL PREPARATION AND TEST PROCEDURE

Sand was placed by air pluviation to achieve a relative density, I_d, of 30%. Selection of this low relative density was based predominately on practical benefits related to sample preparation time, which allowed for a large number of tests to be completed such that a comprehensive study of the mechanisms controlling the response of the piles (e.g. pile installation method, initial safety factor, load redistribution within a pile group) could be accomplished. In addition, the greenfield tests (conducted in a similar way to the tests described by Marshall et al. (2012) and Zhou et al. (2014)) provided data which supplemented existing displacement data for dense (I_d = 90%) and medium-dense (I_d = 60-75%) sands and enabled a fuller understanding of the effects of relative density on tunnelling induced ground deformations (Franza et al. 2018). In series B, C and D, the test procedures may be summarized as follows. [1] After sand pouring, the piles were installed at

$1g$ by jacking to the final embedment depth L_p for non-displacement pile tests and $L_p - 2d_p$ for displacement pile tests. [2] The model was spun to $60g$. [3a] For pile loading tests (series B), piles were jacked while pile head reaction force and settlement were measured. [3b] For displacement pile tests, the piles were jacked in-flight a distance of $2d_p$ and, subsequently, the pile head loads were reduced to the initial service value P_0. [3c] For non-displacement pile tests, the service loads P_0 were directly applied to the piles. The value of the applied service load depended on the specified initial safety factor ($P_0 = Q_0/SF_0$, where Q_0 is the pre-tunnelling ultimate pile capacity and SF_0 is the initial safety factor). For pile groups, the piles were installed sequentially; the installation sequence of displacement piles started from 4 and moved towards 1, whereas the loading sequence of non-displacement piles was pile 1 to 4. [4] For tunnelling beneath piled frame tests, the real-time interface was activated such that the applied loads, P, matched the numerical demand, P'. For tests of single piles, the load demand was maintained constant during the entire tunnelling process (i.e. $P' = P_0$). [5] Small increments of tunnel volume loss ($\Delta V_{l,t} \approx 0.02 - 0.04\%$) were induced and pile settlements were measured. The adopted installation procedures, prior to tunnelling, are able to capture the important features of non-displacement piles (where resistance is mainly provided by the shaft since displacements are insufficient to mobilize base capacity) and displacement piles (where, at the end of the installation, base capacity is mobilized and pile unloading results in negative shaft friction).

TUNNELLING BENEATH SINGLE PILES

Pre-tunnelling load-settlement response

The load capacity of the model piles, Q_0, was required to evaluate the initial safety factor, SF_0, of piles. For non-displacement piles, Q_0 was assumed equal to the load required to push a pile a distance of 10% of the pile diameter, d_p. For displacement piles, Q_0 was evaluated based on the maximum force measured during the jacking of piles in position 2 (discussed below).

The value of Q_0 for non-displacement piles was assessed from the loading tests in series B, where three tests were performed with the same configuration. Results, displayed in Figure 5, show good repeatability, with an average $Q_0 = 740$N at a settlement of $10\%d_p$.

Figure 6 displays the load-normalized settlement curves measured during the installation/loading of the piles in positions 1, 2, and 3 during test series C. Results for non-displacement piles (upper sub-plots) show similar trends in the three different locations. The increase of applied load results in greater pile settlement; however, settlements due to service loads are lower than $10\%d_p$. The displacement pile installations (lower sub-plots) highlight some interesting outcomes. Note that the reference value $Q_0 = 1$kN (shown in Table 1) was measured from tests D2SF1.5 and D2SF2.5 (i.e. piles in position 2). Installations repeated at position 2 gave very similar results, illustrating good repeatability. However, the relative pile-tunnel location had an effect on Q_0, which is neglected by assuming a fixed reference value of Q_0. The value of $Q_0 \approx 1$kN is reasonable for piles in position 3 (tests D3SF1.5 and D3SF2.5, Figure 6(c)). However, piles in position 1 (tests D1SF1.5 and D1SF2.5, Figure 6(a)) were clearly affected by the presence of the model tunnel. The piles in position 1 display a stabilization of the driving load followed by a decrease over the distance of $1 - 2d_p$. This unrealistic response occurs because the tips of piles in position 1 are directly above and very close to the boundary of the water-filled model tunnel.

Tunnelling-induced settlements

In drained conditions, tunnelling can have a reducing effect on the capacity ($\Delta Q < 0$) of nearby piles due to stress relief within the ground. An affected pile will move downwards in an attempt to mobilize the forces (along the shaft and/or at the pile base) necessary to achieve equilibrium. Note that positive shaft friction is mobilized for small magnitudes of relative pile-soil displacements, whereas greater relative movements are needed to fully mobilize base resistance. Displacements will continue to occur as long as the mobilized capacity is lower than the pile load ($Q < P$). For a constant applied load, P, pile failure is initiated when capacity is reduced to the point where it matches the applied load ($Q_{max} \rightarrow P$), potentially inducing large pile movements (Jacobsz et al. 2004; Marshall and Mair 2011). Therefore, in a tunnelling/geotechnical context, the term 'pile failure' should describe the moment when the rate of increase of pile settlement with $V_{l,t}$ shows a significant increase (this definition is adopted within this paper and is referred to as 'geotechnical pile failure'). This framework implies that $SF_0 = Q_0/P$ influences pile failure. However, other

'failure' criteria are also important to consider for practical and/or serviceability reasons (e.g. those related to the superstructure). The arbitrary full-scale displacement of 20mm given by Jacobsz et al. (2004) may be used to define a threshold of 'large' displacements (corresponding to 2.6%d_p for these tests) and the value of 10%d_p is used to refer to 'very large' displacements (relating to performance-based requirements of structures). These thresholds are indicated on subsequent figures for reference.

From test series C, normalized pile displacements (bottom sub-plots) are plotted against $V_{l,t}$ in Figure 7, including shaded lines to indicate 'large' and 'very large' displacements. Greenfield displacements (black lines) at the pile heads and tips are also plotted. Pile displacements in position 3 generally fall within the range defined by the greenfield values at the pile tip and head. However, the piles in positions 1 and 2 diverge from the greenfield displacements from a very low $V_{l,t}$. The rate of displacement is noted to increase with $V_{l,t}$ for piles in positions 1 and 2, whereas it decreases for piles in position 3.

Pile initial safety factor, SF_0, is shown to have a considerable influence on the tunnelling-induced settlements. In each position, the higher the value of SF_0, the lower the pile displacement for both non-displacement and displacement piles. For $SF_0 = 1.5$, the displacement pile in position 1 failed suddenly at $V_{l,t} < 0.5\%$, whereas the non-displacement pile did not show an indication of failure. Displacement and non-displacement piles in position 2 with $SF_0 = 1.5$ display a sharp increase in rate of displacement after $V_{l,t} = 1$ % and 4 %, respectively. The data indicates that $V_{l,t}$ at geotechnical pile failure is higher for non-displacement piles than for displacement piles for a given SF_0 and pile location. This is due to the fact that displacement piles rely on the highly stressed soil regions around their tips for capacity, which are more significantly affected by stress relief caused by tunnel volume loss (due to proximity) than the soil around the shaft (as illustrated by Franza and Marshall (2017) using cavity expansion/contraction analyses).

The data indicate that the 'very large' settlement threshold (10%d_p) should not be used to define an ultimate geotechnical pile failure criterion. For instance, non-displacement piles in positions 1 and 2 have approximately a constant rate of settlement with $V_{l,t}$ even for vertical displacements

greater than this threshold, indicating that a reserve of capacity is available. In these cases, the piles are simply moving with the tunnelling-induced ground displacements, but at a higher rate than greenfield displacements due to the pile loads and the equilibrium condition that requires relative soil-pile settlements to re-mobilize capacity.

Overall, the data indicates that the risk of failure of isolated piles (with constant head loads) located within the tunnel influence zones defined by Jacobsz et al. (2004) (see Figure 1) is low for non-displacement piles but may be an issue for displacement piles. Unfortunately, the acquired data does not enable and assessment of the post-tunnelling safety factor of the piles. This useful information requires considerable testing efforts since a single test is required for each value of tunnel volume loss. This aspect will be the focus of future centrifuge testing at the University of Nottingham.

TUNNELLING BENEATH PILED BUILDINGS

Comparison between greenfield and pile foundation settlements

Firstly, the response to tunnelling of pile foundations subjected to superstructure weight but with a fully-flexible building (i.e. no load redistribution, FR00) is studied and compared with the greenfield data. Initial service loads, P_0, were set equal to 500N, giving $SF_0 = 1.5$ and 2 for non-displacement and displacement piles, respectively.

The installation/loading of the row of piles showed good consistency between tests. The results for displacement piles were similar to those obtained during the installation of the single piles in series C. Non-displacement piles in positions 2, 3, and 4 also generally behaved as the single piles, reaching a final displacement $u_z/d_p \approx 5\%$, as in Figure 6. However, the non-displacement pile in position 1, which was the first in the loading sequence, was affected by the loading of adjacent piles. During its loading to 500N, pile 1 reached a displacement of $u_z/d_p = 5 - 7\%$ (similar to the response of pile 1 in the single pile load tests; Figure 6). After loading the other piles, u_z/d_p of pile 1 reached up to 13%, bringing it closer to the tunnel and therefore more susceptible to the effects of tunnel volume loss. This additional displacement is referred to as 'interaction settlement'

and is discussed in more detail later. Further details on pre-tunnelling installation/loading are given in Franza (2016).

Figure 8 compares settlements from the greenfield test (GF) and tests for non-displacement (NGSF1.5FR00, $SF_0 = 1.5$) and displacement (DGSF2.0FR00, $SF_0 = 2.0$) pile foundations with constant loads (i.e. a fully-flexible superstructure 'FR00' which does not result in pile load redistribution during tunnel volume loss). For clarity, only the displacement pile in position 1 is plotted for DGSF2.0FR00 (explained later). The data shows that non-displacement piles 1 and 2 display settlements considerably larger than the greenfield scenario, whereas piles 3 and 4 settle only slightly more than greenfield surface values. The response of piles outside the tunnel influence zone (piles 3 and 4) does not agree with the outcomes of isolated piles in these positions, in which they settle less than the greenfield surface, as shown in Figure 7 and indicated by Jacobsz et al. (2004). This must be due to the group effect of the four piles. Finally, it is important to note that the non-displacement pile group underwent failure, where the settlement rate with $V_{l,t}$ of pile 1 begins to increases considerably at $V_{l,t} \approx 1\%$ and an unstable condition occurs at $V_{l,t} \approx 1.25\%$. Failure was not observed for pile 1 during the isolated pile test N1SF1.5 (see Figure 7). This disparity between the response of pile 1 in the isolated pile and pile row tests is a result of the difference in the pre-tunnelling state of the ground in the two tests (i.e. because of multiple pile loading and interaction settlements in the pile row test).

The test with a row of displacement piles (DGSF2.0FR00) was terminated at $V_{l,t} \approx 0.2\%$ because of the brittle failure of pile 1. This agrees with the brittle failure of the isolated displacement pile test in position 1 with $SF = 1.5$, shown in Figure 7.

To conclude, Figure 8 illustrates that, for a given scenario, a critical response to tunnelling of both displacement and non-displacement pile foundations is predicted when constant loads are applied (i.e. a hypothetical fully-flexible superstructure). Furthermore, there may be a detrimental group effect on pile post-tunnelling capacity, however further research on this aspect needs to be undertaken given uncertainties related to the effect of the model tunnel on results.

Effect of superstructure stiffness

In this section, the effects of superstructure stiffness on tunnelling-induced pile settlements and load redistribution are investigated. Figure 9 shows the variation of applied load in relation to P_0 (upper plots) and normalized settlements (lower plots) for piles 1 to 4 within the volume loss range $V_{l,t} = 0 - 3\%$. The change of force $\Delta P = P - P_0$ is referred to as the 'superstructure reaction force'. Solid and dashed lines are used to indicate non-displacement and displacement pile foundations, respectively, and a light-to-dark colour transition indicates low to high superstructure stiffness. Note that tests for FR70 were interrupted at lower values of $V_{l,t}$ because they reached an unstable condition within the CCNM application as a consequence of the scaling of signal noise from the centrifuge to the numerical model.

There are two main outcomes that can be gleaned from Figure 9: [i] the superstructure effectiveness in preventing pile failure, and [ii] the complex pattern of load redistribution due to the superstructure. With respect to [i], although $\Delta P/P_0$ of pile 1 is lower than 10% and 20% for displacement and non-displacement pile foundations, respectively, this decrease (due to the superstructure action) is able to prevent geotechnical pile failure, even for the relatively flexible frame FR30. Regarding [ii], the superstructure stiffness redistributes the greatest portion of the total building weight (i.e. the initial load P_0) towards the pile in position 3, whereas the decrease in load of pile 4 is greater than the reduction experienced by pile 1. Furthermore, it can be seen that the structural loads tend towards constant values at volume losses above about 2-3% for the relatively stiff structures FR50 and FR70. These outcomes represent strong evidence of the need to account for the superstructure when undertaking a risk assessment relating to tunnel construction beneath piled foundations.

Superstructure deformation mechanisms

To better understand the mechanisms responsible for the load redistribution, pile head settlement profiles in the direction transverse to the tunnel axis are plotted in Figure 10 at $V_{l,t} = 0.5\%$ and 1.0%. Greenfield vertical displacements at the locations of pile heads and tips are also displayed.

Comparison of the fully flexible (FR00) and rigid (FR70) tests allows identification of the

contribution of superstructure stiffness to settlements. Reaction forces, ΔP, develop as a consequence of the frame resisting bending deformations; they are not caused by tilting because of the implementation of a first-order structural analysis (i.e. neglecting geometric non-linearity). Rigid frames (FR70) constrain the piles to settle such that a straight line profile is formed. In addition, because of the eccentric tunnel-frame location in the tested configurations, rigid frames tilt as well as settle. Therefore, for rigid superstructures, the critical risk may relate to absolute settlements and tilting, rather than bending strains.

It is interesting that the superstructure modification of settlements is qualitatively different for the two pile installation methods, as illustrated in Figure 10(b). Frame reaction forces drive pile 3 into the soil in the case of displacement piles, with little change to the displacements at positions 1 and 4. Whereas for non-displacement pile foundations, distortions are decreased by restraining the downwards movement of piles 1 and 4.

CONCLUSIONS

The following conclusions can be drawn from the present study regarding tunnelling beneath piles and piled buildings in sands.

- The magnitude of tunnelling-induced settlements of piles depends considerably on the pre-tunnelling pile safety factor (SF_0) and pile installation method (displacement/non-displacement piles), as well as on the relative pile-tunnel location. Large pile settlements should be expected for both displacement and non-displacement piles within previously defined tunnel influence zones (Jacobsz et al. 2004). The closer the value of SF_0 to unity, the greater pile settlements will be compared to greenfield values.
- Pile capacity in a tunnel-pile interaction context is generally not well defined. Failure of a pile affected by tunnelling is most commonly based on displacement thresholds, which are certainly applicable, however they do not provide any indication of the actual change in pile load capacity nor the post-tunnelling pile safety factor. The data presented in this paper illustrated how initial safety factor and installation method influence the potential

for 'geotechnical pile failure', which was defined as the tunnel volume loss where a sharp increase in pile displacement was observed. This 'failure' occurs as the pile safety factor approaches unity (due to the effects of tunnel ground loss) and large pile displacements are required to mobilize the loads necessary to achieve equilibrium. The tests presented here did not evaluate the post-tunnelling pile safety factor, an area of interest which will be explored in future research at the University of Nottingham. The topic of how pile capacity should be dealt with in a tunnelling context (and indeed in other related problems such as deep excavations affecting nearby piles) requires further discussion and clarification within the engineering community.

- SF_0 and installation method influence the potential for geotechnical failure of piles within the main tunnel influence area. For a given SF_0, volume loss at geotechnical failure of non-displacement piles is greater than for displacement piles. If service loads are constant, failure is a critical aspect for displacement piles with relatively low SF_0, whereas piles with $SF_0 \geq 2.5$ may not experience geotechnical failure even at high volume losses ($V_{l,t} = 2{-}5\%$).
- Structural stiffness can effectively redistribute building loads among piles. A limited relative reduction in the pile load with volume loss can prevent geotechnical failure of piles directly above the tunnel. The frame action differs between displacement and non-displacement pile foundations in terms of induced pile settlements. Building stiffness can significantly decrease its level of deformation.
- A tunnel-single pile analysis with constant head load conditions (e.g. Marshall and Haji (2015)), which neglects load redistribution due to the structure action, may result in an overly conservative assessment of global tunnel-piled structure interaction.
- The effectiveness of the real-time coupled centrifuge-numerical model was demonstrated for the study of this complex SSI problem. The technique has potential for further analysis of the problem, including the effects of construction phases as well as superstructure non-linearity and damage.

ACKNOWLEDGEMENTS

This work was supported by the Engineering and Physical Sciences Research Council [grant number EP/K023020/1, 1296878, EP/N509620/1]. The authors would like to thank Dr. A. Abdelatif, Dr. C. Heron, Dr. S. Idinyang, and technicians at the Nottingham Centre for Geomechanics (NCG) for their contribution.

REFERENCES

Basile, F. (2014). "Effects of tunnelling on pile foundations." *Soils Found.*, 54(3), 280–295.

Blakeborough, A., Williams, M. S., Darby, A. P., and Williams, D. M. (2001). "The development of real-time substructure testing." *Philos. Trans. R. Soc. A Math. Phys. Eng. Sci.*, 359(1786), 1869–1891.

Devriendt, M. and Williamson, M. (2011). "Validation of methods for assessing tunnelling-induced settlements on piles." *Gr. Eng.*, 25–30.

Dias, T. G. S. and Bezuijen, A. (2015). "Data Analysis of Pile Tunnel Interaction." *J. Geotech. Geoenvironmental Eng.*, 141(12), 04015051.

Franza, A. (2016). "Tunnelling and its effects on piles and piled structures." *Ph.D. Thesis, Univ. Nottingham*.

Franza, A., Idinyang, S., Heron, C., and Marshall, A. M. (2016). "Development of a coupled centrifuge-numerical model to study soil-structure interaction problems." *Proc. 3rd Eur. Conf. Phys. Model. Geotech. (Eurofuge 2016)*, L. Thorel, A. Bretschneider, M. Blanc, and S. Escoffier, eds., Nantes, France, 135–140.

Franza, A. and Marshall, A. (2017). "Centrifuge modelling of tunnelling beneath axially loaded displacement and non-displacement piles in sand." *Proc. Geotech. Front. 2017. GSP 277 Transp. Facil. Struct. site Investig.*, T. L. Brandon and R. J. Valentine, eds., Orlando, Florida, 576–586.

Franza, A. and Marshall, A. M. (2018). "Centrifuge Modeling Study of the Response of Piled Structures to Tunneling." *J. Geotech. Geoenvironmental Eng.*, 144(2), 04017109.

Franza, A., Marshall, A. M., Haji, T., Abdelatif, A. O., Carbonari, S., and Morici, M. (2017). "A

simplified elastic analysis of tunnel-piled structure interaction." *Tunn. Undergr. Sp. Technol.*, 61, 104–121.

Franza, A., Marshall, A. M., and Zhou, B. (2018). "Greenfield tunnelling in sands: the effects of soil density and relative depth." *Geotechnique*, DOI:10.1680/jgeot.17.p.091.

Hong, Y., Soomro, M., and Ng, C. (2015). "Settlement and load transfer mechanism of pile group due to side-by-side twin tunnelling." *Comput. Geotech.*, 64, 105–119.

Idinyang, S., Franza, A., Heron, C. M., and Marshall, A. M. (2018). "Real-time data coupling for hybrid testing in a geotechnical centrifuge." *International Journal of Physical Modelling in Geotechnics*, DOI:10.1680/jphmg.17.00063.

Jacobsz, S. W., Standing, J. R., Mair, R. J., Hagiwara, T., and Sugiyama, T. (2004). "Centrifuge modelling of tunnelling near driven piles." *Soils Found.*, 44(1), 49–56.

Kong, V., Cassidy, M. J., and Gaudin, C. (2015). "Development of a real-time hybrid testing method in a centrifuge." *Int. J. Phys. Model. Geotech.*, 15(4), 169–190.

Lee, C.-J. J. and Chiang, K.-H. H. (2007). "Responses of single piles to tunneling-induced soil movements in sandy ground." *Can. Geotech. J.*, 44(10), 1224–1241.

Loganathan, N., Poulos, H. G., and Stewart, D. P. (2000). "Centrifuge model testing of tunnelling-induced ground and pile deformations." *Géotechnique*, 50(3), 283–294.

Marshall, A. (2012). "Tunnel-Pile Interaction Analysis Using Cavity Expansion Methods." *J. Geotech. Geoenviromental Eng.*, (October), 1237–1246.

Marshall, A. and Mair, R. (2011). "Tunneling beneath driven or jacked end-bearing piles in sand." *Can. Geotech. J.*, 48(12), 1757–1771.

Marshall, A. M., Farrell, R., Klar, A., and Mair, R. (2012). "Tunnels in sands: the effect of size, depth and volume loss on greenfield displacements." *Géotechnique*, 62(5), 385–399.

Marshall, A. M. and Haji, T. (2015). "An analytical study of tunnel-pile interaction." *Tunn. Undergr. Sp. Technol.*, 45, 43–51.

Ng, C., Soomro, M., and Hong, Y. (2014). "Three-dimensional centrifuge modelling of pile group responses to side-by-side twin tunnelling." *Tunn. Undergr. Sp. Technol.*, 43, 350–361.

Ng, C. W. W., Lu, H., and Peng, S. Y. (2013). "Three-dimensional centrifuge modelling of the effects of twin tunnelling on an existing pile." *Tunn. Undergr. Sp. Technol.*, 35, 189–199.

Selemetas, D. and Standing, J. R. (2017). "Response of Full-Scale Piles to EPBM Tunnelling in London Clay." *Géotechnique*, 67(9), 823–836.

Soomro, M. A., Hong, Y., Ng, C. W. W., Lu, H., and Peng, S. (2015). "Load transfer mechanism in pile group due to single tunnel advancement in stiff clay." *Tunn. Undergr. Sp. Technol.*, 45, 63–72.

White, D., Take, W., and Bolton, M. (2003). "Soil deformation measurement using particle image velocimetry (PIV) and photogrammetry." *Géotechnique*, 53(7), 619–631.

Williamson, M. G., Elshafie, M. Z. E. B., Mair, R. J., and Devriendt, M. D. (2017a). "Open-face tunnelling effects on non-displacement piles in clay – part 1: centrifuge modelling techniques." *Géotechnique*, 67(11), 983–1000.

Williamson, M. G., Mair, R. J., Devriendt, M. D., and Elshafie, M. Z. E. B. (2017b). "Open-face tunnelling effects on non-displacement piles in clay – part 2: tunnelling beneath loaded piles and analytical modelling." *Géotechnique*, 67(11), 1001–1019.

Zhang, R., Zheng, J., Pu, H., and Zhang, L. (2011). "Analysis of excavation-induced responses of loaded pile foundations considering unloading effect." *Tunn. Undergr. Sp. Technol.*, 26(2), 320–335.

Zhou, B., Marshall, A. M., and Yu, H.-S. (2014). "Effect of relative density on settlements above tunnels in sands." *2014 GeoShanghai Int. Congr. Tunneling Undergr. Constr.*, Vol. 242 GSP, Shanghai, China, American Society of Civil Engineers, 96–105.

List of Tables

TABLE 1. Summary, in model scale dimensions, of centrifuge experiments.

Test series	Label (# tests performed)		Pile type †	Position #	Offset x (mm)	Serv. Load P_0 (N)	Capacity‡ Q_0 (N)	SF_0 (-)	Note§
A	GF	(1)	-	-	-	-	-	-	Greenfield
B	LP	(3)	N	3	150	-	-	-	Loading
C	N1SF1.5	(1)	N	1	0	493	740	1.5	TPI
C	N1SF2.5	(1)	N	1	0	296	740	2.5	TPI
C	D1SF1.5	(1)	D	1	0	667	1000	1.5	TPI
C	D1SF2.5	(1)	D	1	0	400	1000	2.5	TPI
C	N2SF1.5	(1)	N	2	75	493	740	1.5	TPI
C	N2SF2.5	(1)	N	2	75	296	740	2.5	TPI
C	D2SF1.5	(1)	D	2	75	667	1000	1.5	TPI
C	D2SF2.5	(1)	D	2	75	400	1000	2.5	TPI
C	N3SF1.5	(1)	N	3	150	493	740	1.5	TPI
C	N3SF2.5	(1)	N	3	150	296	740	2.5	TPI
C	D3SF1.5	(1)	D	3	150	667	1000	1.5	TPI
C	D3SF2.5	(1)	D	3	150	400	1000	2.5	TPI
D	NGSF1.5FR00	(1)	N	1-4	0-225	500	740	1.5	TPGI
D	NGSF1.5FR30	(1)	N	1-4	0-225	500	740	1.5	TPSI
D	NGSF1.5FR50	(1)	N	1-4	0-225	500	740	1.5	TPSI
D	NGSF1.5FR70	(1)	N	1-4	0-225	500	740	1.5	TPSI
D	DGSF2.0FR00	(1)	D	1-4	0-225	500	1000	2.0	TPGI
D	DGSF2.0FR30	(1)	D	1-4	0-225	500	1000	2.0	TPSI
D	DGSF2.0FR50	(1)	D	1-4	0-225	500	1000	2.0	TPSI
D	DGSF2.0FR70	(1)	D	1-4	0-225	500	1000	2.0	TPSI

† N: non-displacement piles; D: displacement piles

‡ The reported values do not account for the influence of the pile offset

§ TPI = tunnel-pile interaction, TPGI = tunnel-pile group interaction, TPSI = tunnel-pile-structure interaction

List of Figures

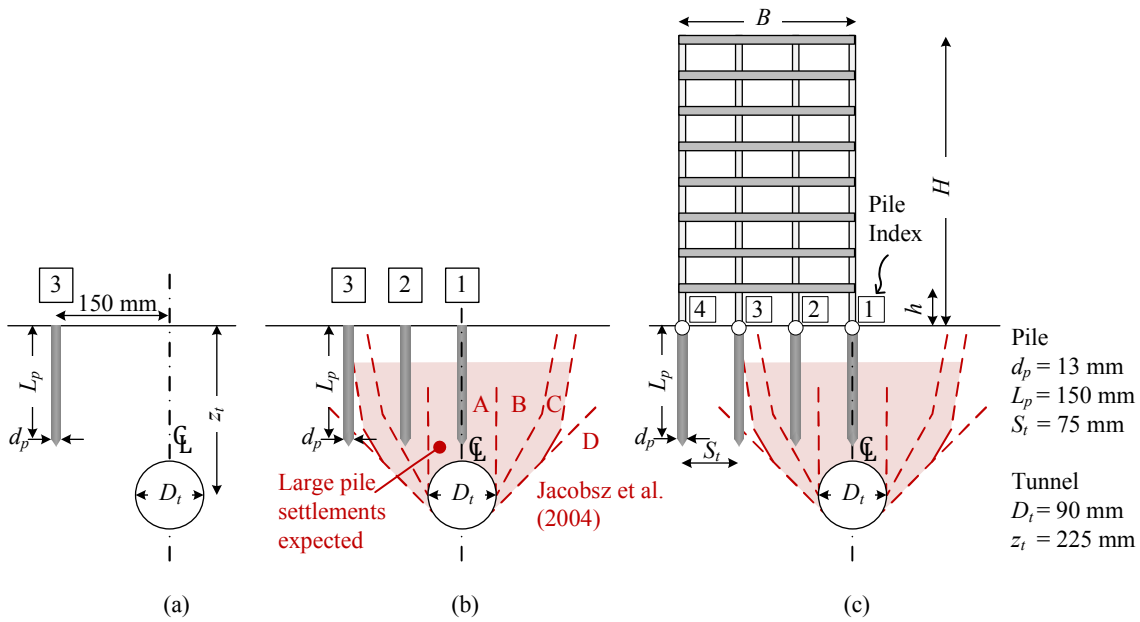

Fig. 1. Test layout (in model scale): (a) loading tests, (b) tunnelling beneath a single pile (showing locations of piles; only single pile installed for each test), and (c) tunnelling beneath a piled frame (using the CCNM technique).

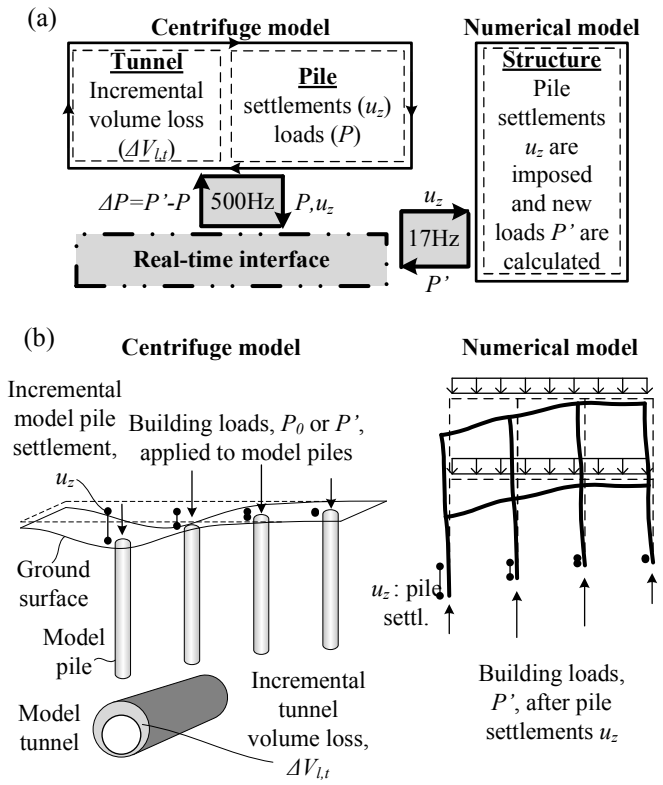

Fig. 2. Coupled centrifuge-numerical model: (a) diagram of the coupling loop, (b) de-coupled geotechnical and structural domains.

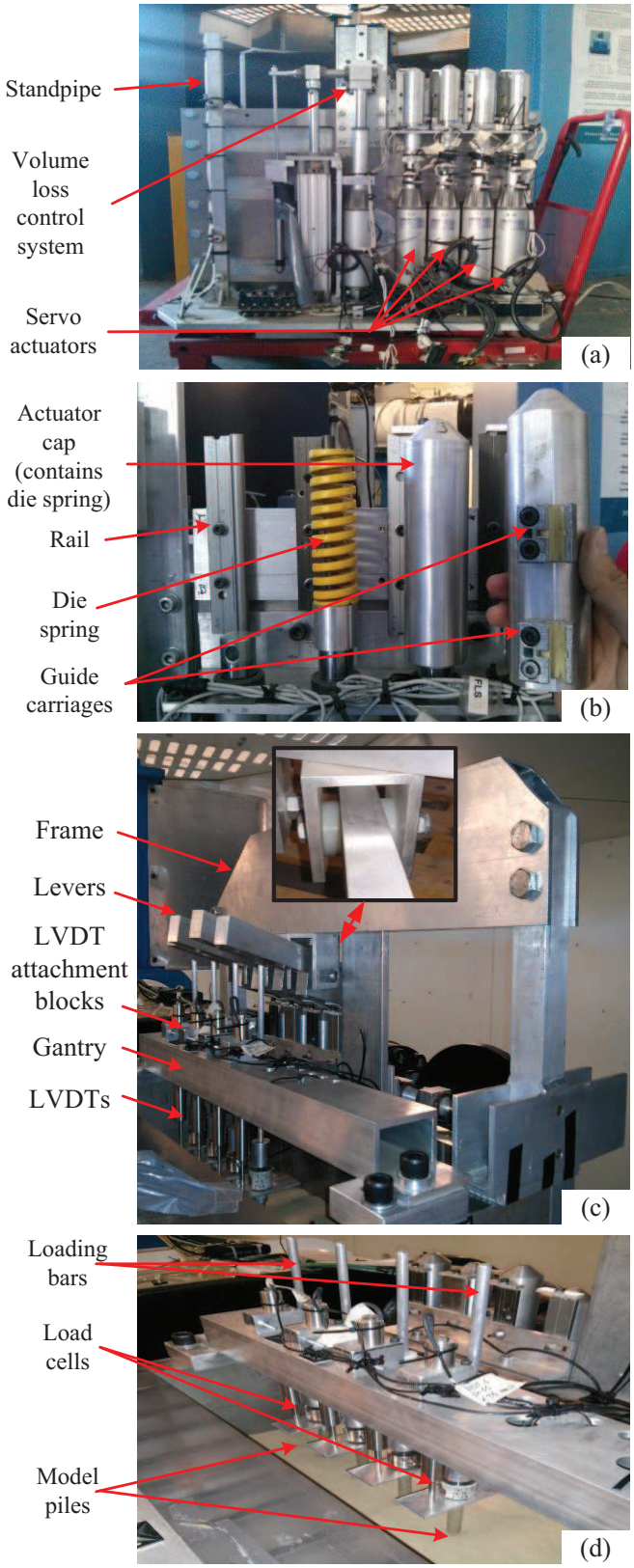

Fig. 3. (a) Back view of the package, (b) details of the actuator caps, (c) front views of the lever system, and (d) view of the model pile foundation.

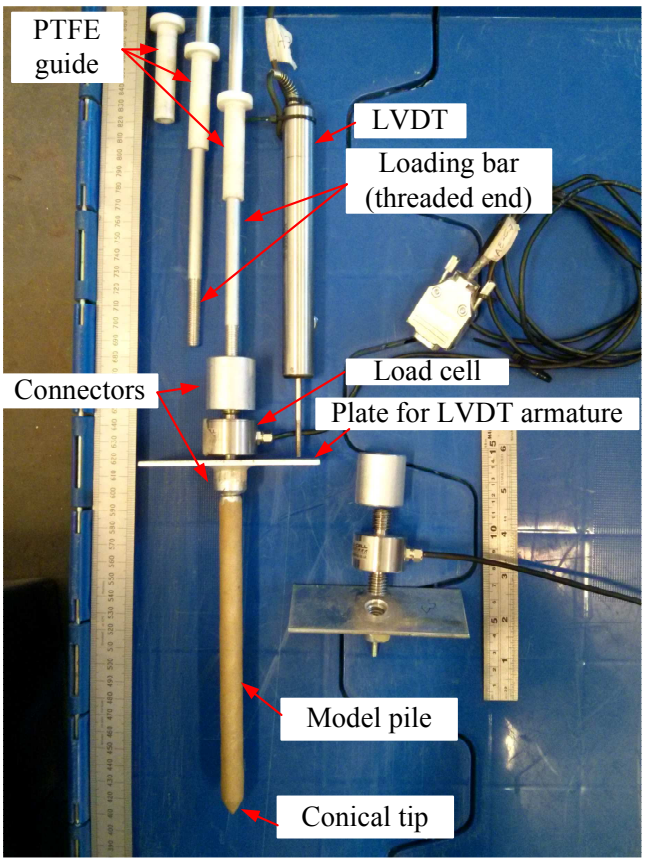

Fig. 4. Model pile and pile cap.

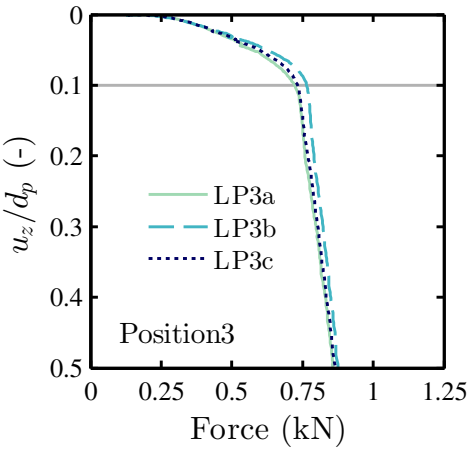

Fig. 5. Pile loading tests (LP) for non-displacement piles (position 3).

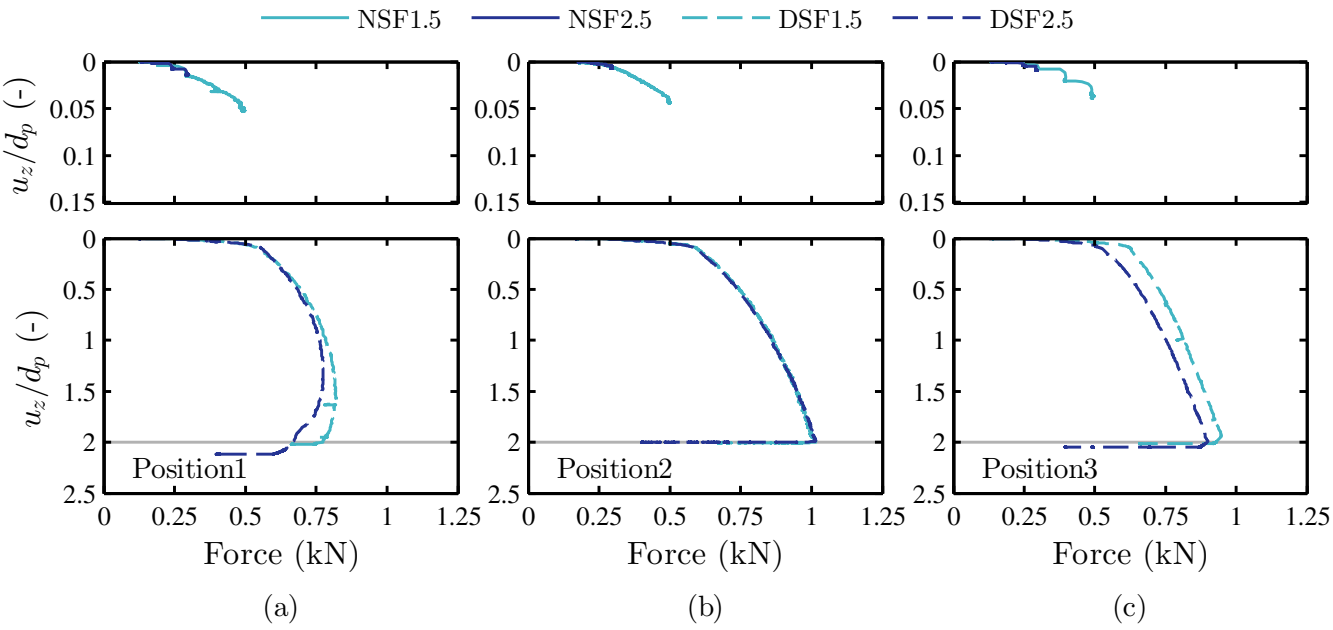

Fig. 6. Load versus normalised settlement curves during pile installation/loading for non-displacement piles (top) and displacement piles (bottom) in positions (a) 1, (b) 2, and (c) 3 during test series C.

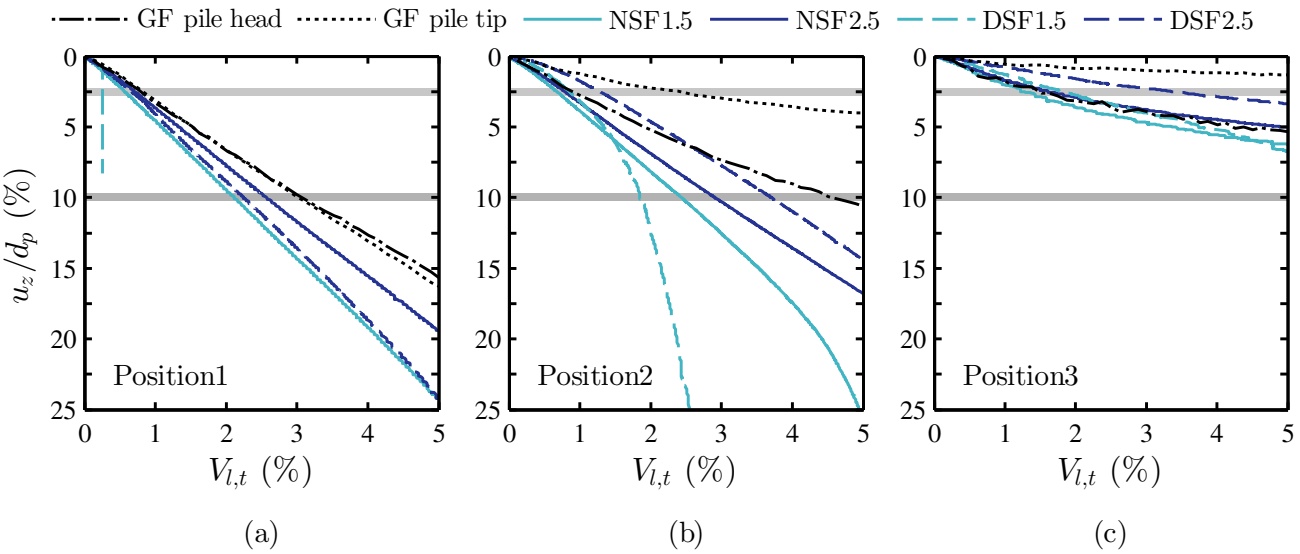

Fig. 7. Normalised settlement during tunnelling beneath single non-displacement and displacement piles in positions (a) 1, (b) 2, and (c) 3.

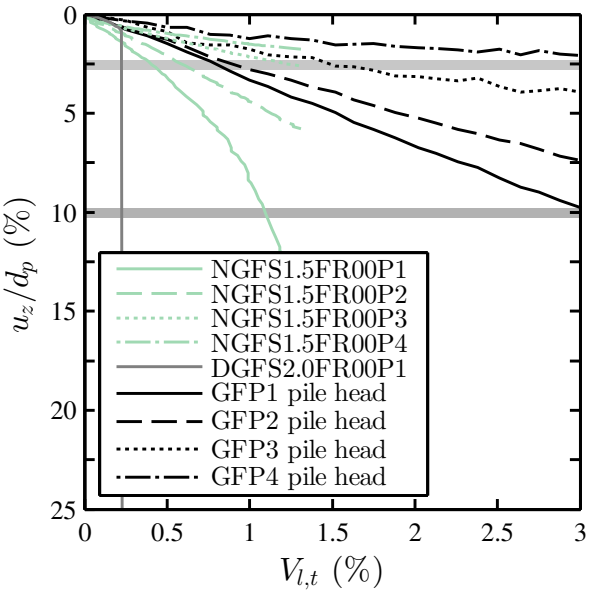

Fig. 8. Tunnelling-induced greenfield and pile row settlements for non-displacement and displacement pile foundations with constant head loads.

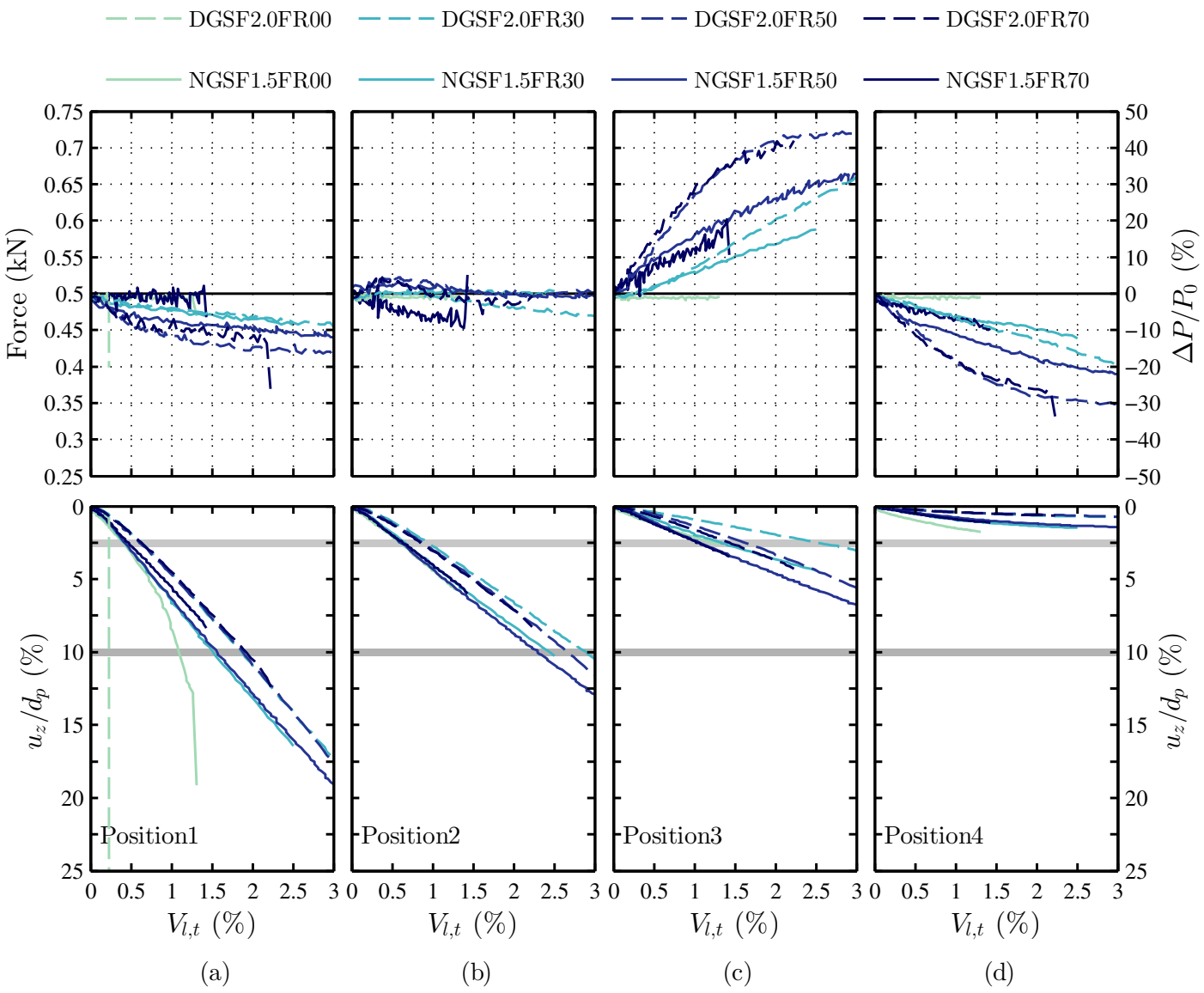

Fig. 9. Variation of tunnelling-induced pile settlements and load distributions with frame stiffness: piles in positions (a) 1, (b) 2, (c) 3, and (d) 4.

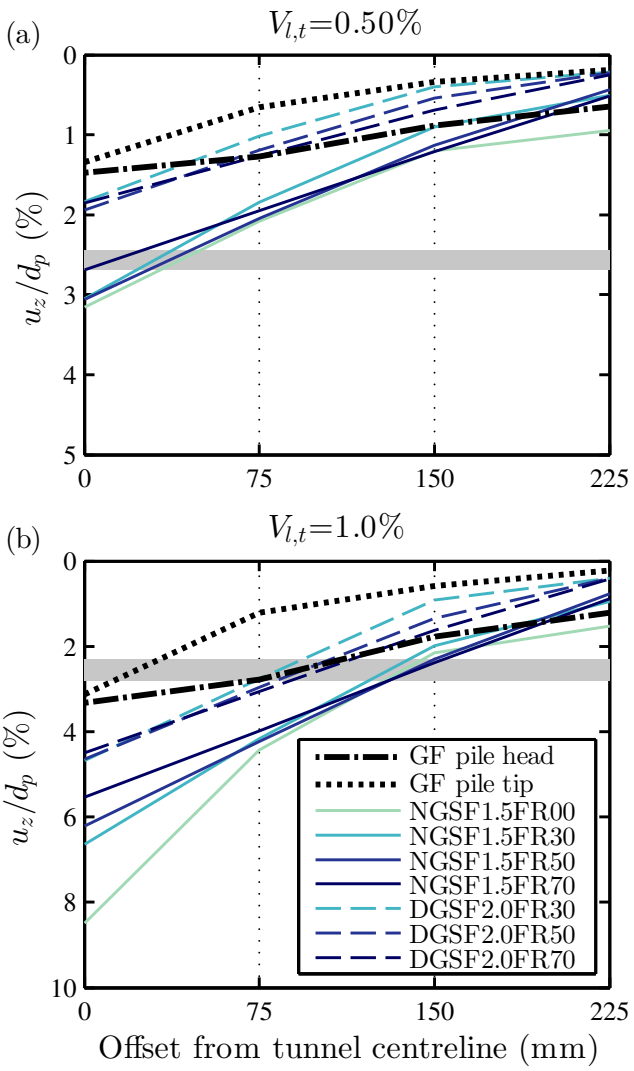

Fig. 10. Greenfield and frame base settlements.